SELF-ADAPTIVE EDGE-PRESERVING SMOOTHING AND ITS APPLICATIONS IN SEISMIC IMPEDANCE INTERPRETATION

RONG-HUO DAI[1], YU-PEI ZHANG[2], FAN-CHANG ZHANG[3] and CHENG YIN[4]

[1] *School of Mathematics & Information, China West Normal University, Nanchong 637002, P.R. China. daironghuo@yeah.net*
[2] *Research Center of Exploration and Development Technology, Yanchang Oilfield Company, Yan'an 716099, P.R. China.*
[3] *School of Geosciences, China University of Petroleum (East China), Qingdao 266580, P.R. China.*
[4] *School of Geoscience and Technology, Southwest Petroleum University, Chengdu 610500, P.R. China.*

(Received August 8, 2019; revised version accepted May 8, 2021)

ABSTRACT

Dai, R.-H., Zhang, Y.-P., Zhang, F.-C. and Yin, C., 2121. Self-adaptive edge-preserving smoothing and its applications in seismic impedance interpretation. *Journal of Seismic Exploration*, 30: 303-318.

Seismic attributes, such as seismic impedance, AVO or AVA attributes, or other amplitude-like attributes, and so forth, increase the geological information interpretation ability of seismic data. However, in practical case, the calculation of seismic attributes is based on the mathematical formula, such as derivative or integration of seismic data. So, it also enhances random noise. Edge-preserving smoothing (EPS) method can suppress random noise along reflectors while preserving major stratigraphic or structural discontinuities features. These features are very important for seismic data's geological interpretaion. However, the conventional EPS filter use fixed filter window size to perform in practice. Hence, the little geological features (e.g., channels, minor fault or thin layers) will be suppressed if their width are smaller than used filter window size. On the other hand, if the filter window size is too small, noise will not be removed sufficiently. In order to overcome this issue, we present a new EPS filter which uses a series of different window size and self-adaptively chooses the best one through filter window size scanning. The self-adpative EPS filter can strike a balance between noise remove and useful geological information protection. Applications on model tests and real data examples have shown the effectivity of the proposed method.

KEY WORDS: self-adaptive edge-preserving smoothing, impedance interpretation, filter window size scanning, seismic attributes.

0963-0651/21/$5.00

INTRODUCTION

Geophysicists and geologists use the lineaments with meaningful geological features in seismic data cubes to predict oil or gas reservoirs. These seismic data cubes include seismic impedance (AlBinHassan et al., 2006; Zhang et al., 2014, 2015a; Dai et al., 2016), amplitude gradients (Luo et al., 2002), volumetric curvatures (Al-Dossary and Marfurt, 2006; Wang et al., 2012), AVO or AVA attribute (Dai et al., 2014a, 2014b, 2015; Zhang et al., 2015b; Zhang and Dai, 2016), and so forth. They are also called seismic attributes, which are related to the reservoir rock physics characteristics (Ba et al., 2017, 2018; Pang et al., 2019). Hence, it is the key of seismic interpretation.

A big problem in the application of these seismic attributes is the effect of random noise. The calculation of seismic attributes is based on the different mathematical formula. For example, the impedance attrinutes are integration of seismic data. It will also enhance random noise, which can obscure the geological lineaments, such as the edges of geological feature (Hocker and Fehmers, 2002; Fehmers and Hocker, 2003; Al-Dossary and Marfurt, 2007). The quality of such edges and lineaments is directly related to the effectiveness of noise-removing filter.

In the existing literatures, many linear or nonlinear filters have been broadly used to remove noise and improve the interpretability of seismic attributes (Al-Dossary and Marfurt, 2007; Liu et al., 2009a; Liu and Luo, 2012). In order to suppress noise while preserve the edges of geologic feature, Luo et al., (2002) proposed the edge-preserving smoothing (EPS) filter. It attemps to overcome the conflict between edge preserving and noise suppression through a modification of running average smoothing alogrithm.

EPS filter has been successfully applied to many seismic data cubes. Luo et al., (2002) used EPS filter in seismic amplitude attributes to suppress noise. Then, Al-Dossary et al., (2002) used 3D EPS filter to perform seismic edge detection. AlBinHassan et al., (2006) used 2D and 3D EPS filter to enhance the structure features in seismic impedance cubes. Marfurt (2006) combined the multiwindow dip search, principal component filter and EPS fitler to estimate 3D reflector dip and azimuth. Misra and Sacchi (2008) used EPS filter in AVO attributes inversion to reduce random noise in pre-stack seismic data. Al-Dossary and Wang (2011) used 3D EPS filter in seismic attributes to implement many tasks, such as random noise remove, footprints reduction, faults and unconformities identification and curvature attributes enhancement. Halpert (2012) used EPS filter to segment seismic images. Zhang et al. (2015a) used EPS filter as a regularization method in seismic impedance inversion to better reflect the changes of stratum.

However, the filter window size of the conventional EPS filter is fixed. Hence, the little geologic features smaller than the window size will be suppressed (Luo et al., 2002; Al-Dossary and Marfurt, 2007; Zhang et al.,

2015a). The subsurface is so complicated and there are typically features with a range of thickness. If the filter window size is too small, random noise will not be sufficiently removed. To sovle this issue, we propose an self-adaptive EPS (SA-EPS) filter. This proposed SA-EPS filter is performed on model and real seismic data to demonstrate its feasibility.

METHODS

EPS filter

EPS attempts to look for the most homogeneous fragment around a sample to be filtered in an input data set, calculate the average value of the most homogeneous fragment and assign the average value to that sample (Luo et al., 2002; Al-Dossary and Marfurt, 2007; Al-Shuhail and Al-Dossary, 2020). It has been used to remove random noise in seismic impedance data while preserve stratigraphic discontinuities (i.e., edges of geologic bodies) (AlBinHassan et al., 2006).

An example of 1D 5-point EPS filter is designed in Fig. 1, where a data set with M model parameters around m_i to be filtered is shown. First, five 5-point windows are chosen around m_i, and the standard deviations for each window are calculated. The one with the least standard deviation is selected as the most homogeneous fragment of these array windows (We call this least standard deviation as window factor). Next, the sample m_i is replaced with the average value of the most homogenous window. Then, the array of windows move along the entire length of data set and the same procedure is repeated at each sample. At last, the result is EPS filter output.

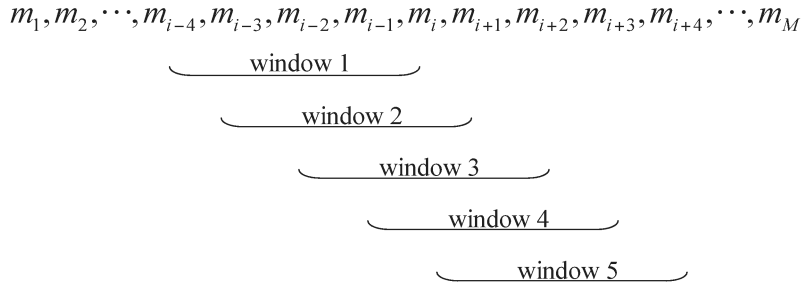

Fig. 1. Design of 5-point EPS filter around sample m_i to be filtered.

For n-point EPS filter, we will get n n-point windows and n standard deviations for each sample to be filtered and one most homogenous window. 1D EPS filter can be generalized to 2D and 3D (AlBinHassan et al., 2006).

Fig. 2 shows a comparison between the actions of running-average smoothing filter (one kind of mean filter) and EPS filter on a 1D impedance model with two sharp edges. Fig. 2a shows the real 1D impedance model.

Fig. 2b shows the same impedance model with random noise which obscures sharp edges. Fig. 2c shows the result of running-average smoothing filter on the noise-contaminated model. Fig. 2d shows the result of a 7-point EPS filter on the noise-contaminated model. We can see that, the running-average smoothing filter can effectively reduce much noise, but it cannot preserve sharp edges; compared to running-average smoothing filter, EPS filter can both effectively suppress random noise and preserve sharp edges.

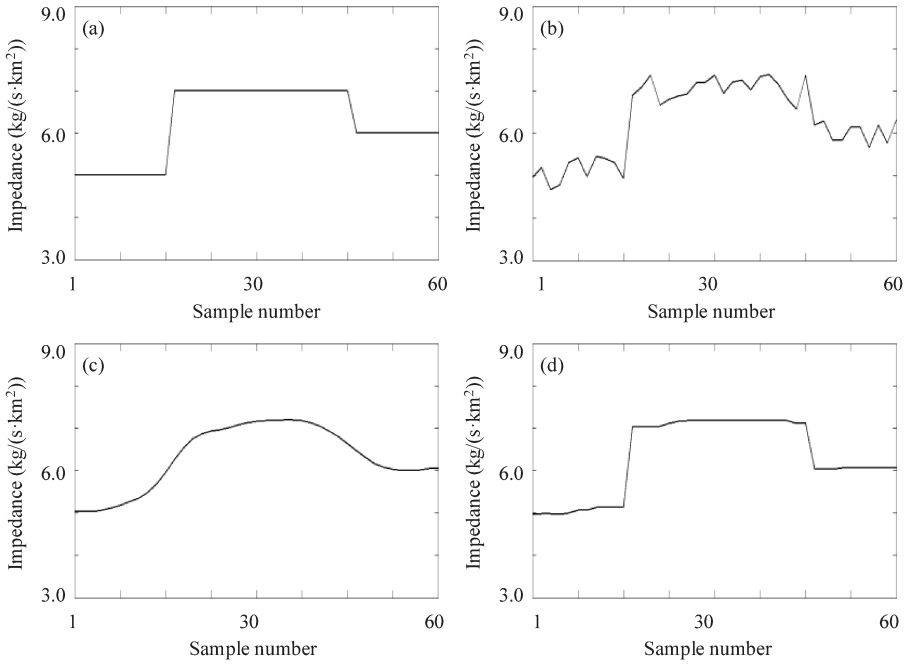

Fig. 2. Comparison between the actions of running-average smoothing filter (one kind of mean filter) and EPS filter. (a) The real 1D impedance model with two sharp edges. (b) The impedance model with random noise which obscures sharp edges. (c) The result of running-average smoothing filter on the noise-contaminated model. (d) The result of 7-point EPS filter on the noise-contaminated model.

Defect of conventional EPS

From the above texts, we see that the filter window size of EPS filter is fixed. The little geologic features (e.g., channels, tiny fault or thin layers) smaller than the filter window size will be suppressed (Luo et al., 2002; Al-Dossary and Marfurt, 2007; Zhang et al., 2015b). On the other hand, if the window size is too small, random noise will not be sufficiently removed. The subsurface is so complicated and there are typically features with a range of thickness. If a fixed window is used, there is a trade-off between noise remove and small geologic features preservation.

We use a 1D impedance model shown in Fig. 3a to reveal this trade-off of conventional EPS filter. This model contains two layers with different thickness. Fig. 3b shows the same model with random noise. First, a 4-point EPS filter is performed on the noise-contaminated model and the result is shown in Fig. 3c. We can see that random noise at thinner layer is suppressed. However, random noise at thicker layer is not sufficiently removed. Next, an 11-point EPS filter is performed on the noise-contaminated model and the result is shown in Fig. 3d. We can see that random noise is sufficiently removed in both thick and thin layer. However, the edges of thinner layer are fully suppressed.

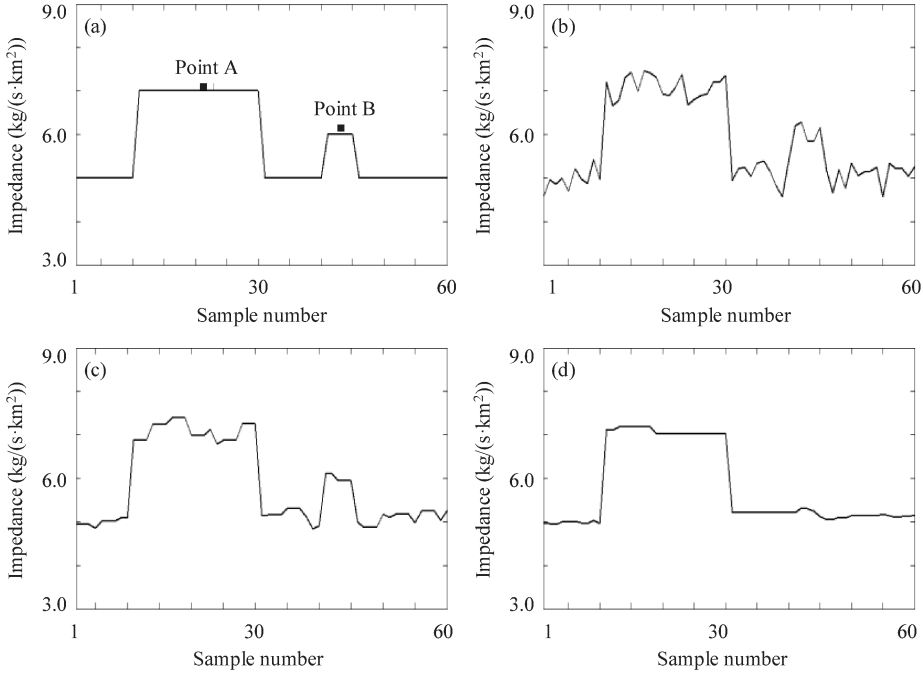

Fig. 3. Comparison between the actions of different point EPS filter. (a) The real 1D impedance model. (b) The impedance model with random noise. (c) The result of 4-point EPS filter on the noise-contaminated model. (d) The result of 11-point EPS filter on the noise-contaminated model.

SA-EPS filter

An unsuitable choice of filter window size will suppress some little geologic features, or do not sufficiently remove random noise. To solve this issue, we propose a self-adaptive edge-preserving smoothing (SA-EPS) filter through filter window size scanning.

Two figures are employed to show the principle of window size scanning. First, two samples are chosen (sample A and sample B in Fig. 3a). These

two points locate at different layers with different thickness. Sample A locates at the thicker layer and sample B locates at thinner layer. A series of EPS filters with different filter window size are performed on the two samples. Record the window factors (i.e., least standard deviation for each filter window size). The results are shown in Fig. 4. We can see that, the window factors for different filter window sizes are different. For sample A, 10-point EPS filter has the smallest window factor. On the other hand, for sample B, small point EPS filters have smaller window factors. Hence, one can use filter window size scanning to self-adaptively choose the best filter window size for each sample to be filtered.

Based on the above contents, the workflow of SA-EPS is as follows. First, perform a series of EPS filters with a different filter window size at the sample to be filtered. For example, we can apply 4-point to 21-point filter to the model shown in Fig. 3. EPS filter with very small window size is no use. Hence, the window size of less than 3 is not considered. Then, calculate the window factors for each EPS filter and find the smallest one. The one with the smallest window factor is chosen as the EPS filter with the best-fitting window size for that sample. Next, replace that sample by the value of the best-fitting EPS filter result. Finally, repeat the above procedure at each sample to obtain the final SA-EPS filter output.

From the workflow of the SA-EPS filter, we can see that it is nothing but an additional step of filter window size scanning before the procedure of the conventional EPS filter. The filter window size scanning is used to self-adaptively find the best fitting window size for each sample to be filtered.

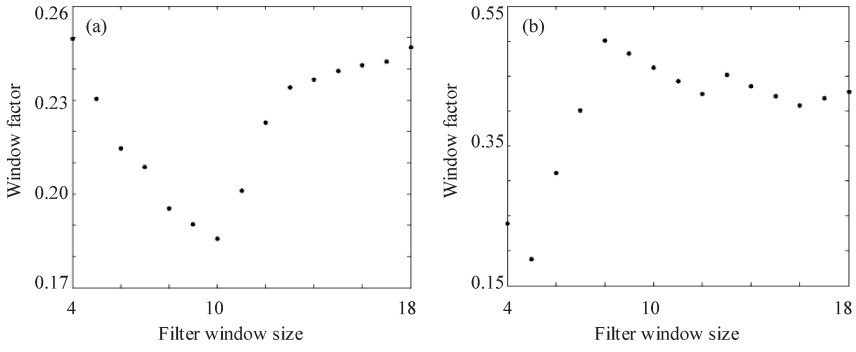

Fig. 4. Window factor versus with filter window size. (a) For sample A shown in Fig. 3a. (b) For sample B shown in Fig. 3a.

Fast EPS algorithm

From the workflow of SA-EPS filter, the realization of SA-EPS filter is very time consuming. So, a fast EPS algorithm is proposed to accelerate the computation speed.

We use a 1D 5-point EPS filter to show the principle of fast EPS algorithm. Fig. 5 shows a vector with 9 samples around the m_5 to be filtered. In the process of EPS filter, we will calculate five average values and standard deviations around m_5 (i.e. the average values and standard deviations for window 1, 2, 3, 4, and 5 shown in Fig. 5.). We notate $\mathbf{E}_n$ and $\mathbf{D}_n$ (n = 1, 2, 3, 4, and 5) as the average value and standard deviation for each window. So,

$$\mathbf{E}_1 = \frac{1}{5}(m_1 + m_2 + m_3 + m_4 + m_5) \quad , \tag{1}$$

$$\mathbf{D}_1 = [\frac{1}{5}\sum_{i=1}^{5}(m_i - \mathbf{E}_1)^2]^{1/2}, \tag{2}$$

$$\mathbf{E}_2 = \frac{1}{5}(m_2 + m_3 + m_4 + m_5 + m_6) \quad , \tag{3}$$

$$\mathbf{D}_2 = [\frac{1}{5}\sum_{i=2}^{6}(m_i - \mathbf{E}_2)^2]^{1/2}, \tag{4}$$

and so forth.

In routine EPS filter, it calculates average value and standard deviation for each window, separately. However, in fast EPS algorithm, we establish the relation between two adjacent windows. For example, with $\mathbf{E}_1$, $\mathbf{E}_2$, $\mathbf{D}_1$, and $\mathbf{D}_2$, from mathematical relation, we have,

$$5\mathbf{E}_2 = m_2 + m_3 + m_4 + m_5 + m_6 = 5\mathbf{E}_1 + (m_6 - m_1), \tag{5}$$

$$5\mathbf{D}_2^{\,2} = \sum_{i=2}^{6}(m_i - \mathbf{E}_2)^2 = 5\mathbf{D}_1^{\,2} - \frac{(m_6 - m_1)^2}{5} + (m_6 - m_1)\cdot(m_6 + m_1 - 2\mathbf{E}_1) \tag{6}$$

Let $t = \dfrac{m_6 - m_1}{5}$ and then have the follow equations,

$$\mathbf{E}_2 = \mathbf{E}_1 + t \quad , \tag{7}$$

$$\mathbf{D}_2^{\,2} = \mathbf{D}_1^{\,2} - t^2 + t(m_6 + m_1 - 2\mathbf{E}_1) \quad . \tag{8}$$

The same relation can be generalized to the other adjacent windows. Hence, the average value and standard deviation of next window can be calculated through the average value and standard deviation of last window. Through the relation between two adjacent windows, the computation speed of EPS filter is accelerated.

In addition, when perform EPS filter at m_6, there are four windows same as m_5. Hence, it just needs to calculate only one new average value and one new standard deviation. It is also accelerate the computation speed.

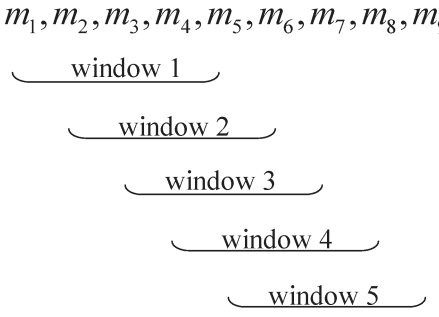

Fig. 5. Design of 5-point EPS filter around m_5 to be filtered.

MODEL TESTS

We use the 1D impedance model shown in Fig. 3 to show the feasibility of the SA-EPS filter. Fig. 6a shows the same 1D impedance model shown in Fig. 3. Then, the SA-EPS filter is performed on the noise-contaminated model shown in Fig. 3b and the result is shown in Fig. 6b. We can see that random noise is fully removed and sharp edges are preserved in both thick and thin layers.

To quantitatively show the effectiveness of SA-EPS, we calculate the relative errors (RE) for different filter results. The RE is calculated by the following equation,

$$\mathrm{RE}=\frac{\|\hat{\mathbf{m}}-\mathbf{m}\|_2^2}{\|\mathbf{m}\|_2^2}, \tag{9}$$

where $\mathbf{m}$ is the noise-free model, $\hat{\mathbf{m}}$ is the filtered results. The REs for different filter results shown in Fig. 3c, Fig. 3d and Fig. 6b are shown in Table 1. We can see that, the RE for SA-EPS is smallest.

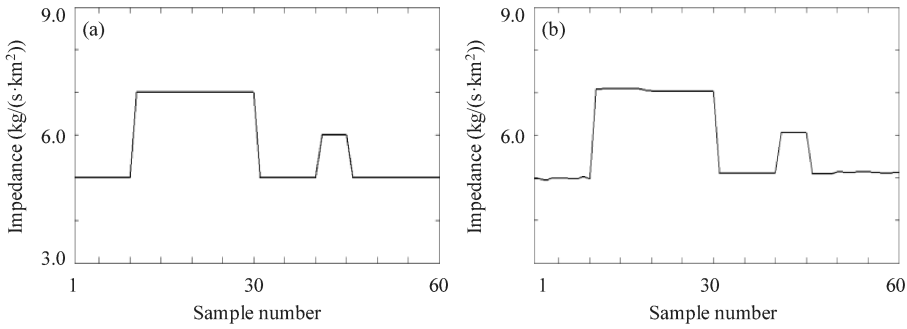

Fig. 6. Comparison between the result of SA-EPS filter and real 1-D impedance model. (a) The same impedance model shown in Fig. 3a. (b) The result of SA-EPS filter performed on the noise-contaminated model shown in Fig. 3b.

Table 1. The REs for different filter results in the case of 1D impedance model.

Filter	RE
4-point EPS	0.1257
11-point EPS	0.1001
SA-EPS	0.0270

To further show the feasibility of SA-EPS in complicated geologic features, we perform a 2D impedance model test. The true impedance model section is shown in Fig. 7a and its corresponding noise-contaminated is shown in Fig. 7b, which contains 20% Gaussian random noise.

Then, the conventional 11-point EPS filter is performed on the noise-contaminated model. The filter result is shown in Fig. 8a. From the comparison between Figs. 7a and 8a, we can see that the filter result through 11-point EPS is basically consistent with the true impedance model. However, many little geologic features are suppressed. Next, SA-EPS filter is performed on the noise-contaminated model and the filter result is shown in Fig. 8b. From the comparison between Fig. 7a and Fig. 8b, we can see that SA-EPS filter gives a better result with less discordance compared to the conventional EPS filter. The interfaces of layers and edges of lenticular bodies in Fig. 8b are very clear (e.g. the edges of lenticular bodies within white ovals).

In addition, we calculate REs for different filter results and list the results in Table 2. We can see that, the RE for SA-EPS is smaller than EPS.

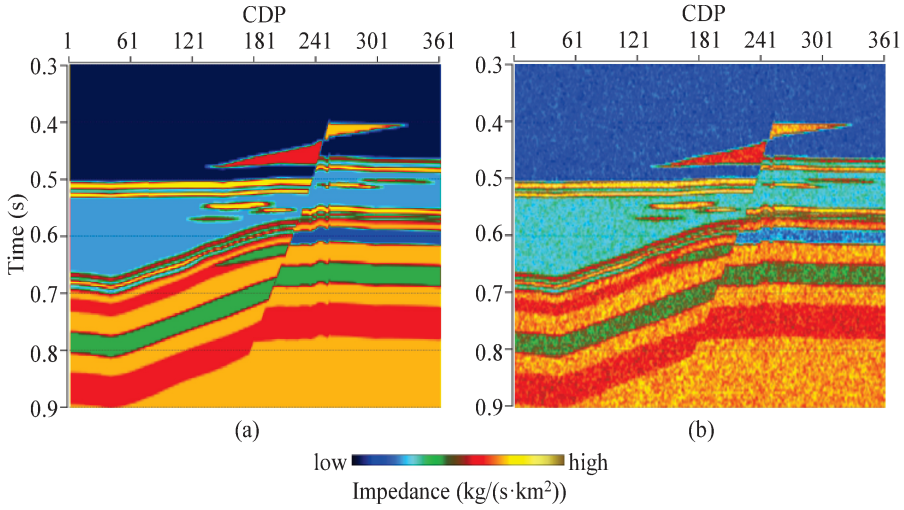

Fig. 7. (a) The real 2-D impedance model. (b) The impedance model with random noise.

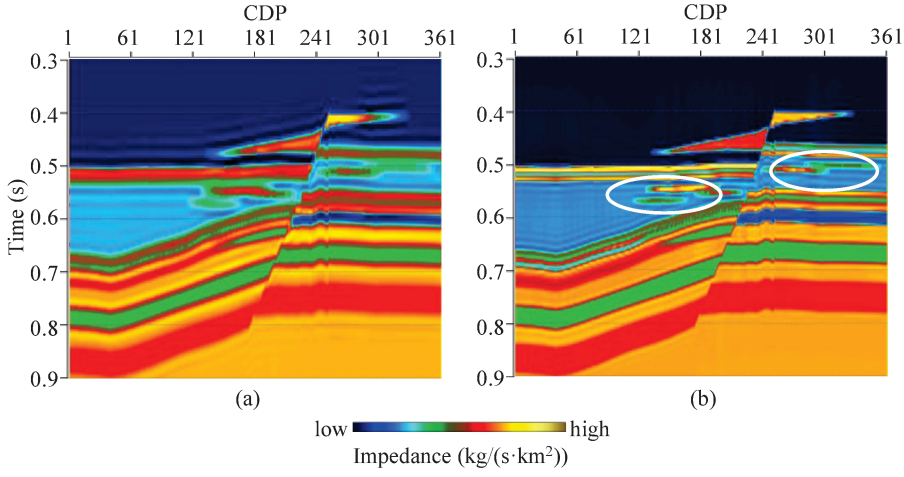

Fig. 8. Comparison between SA-EPS filter and conventional EPS filter on the 2D impedance model. (a) The filter result of 11-point EPS. (b) The filter result of the SA-EPS.

Table 2. The REs for different filter results in the case of the 2D impedance model.

Filter	RE
EPS	0.1508
SA-EPS	0.0781

APPLICATIONS ON REAL SEISMIC IMPEDANCE DATA

There are many reasons motivated us to apply SA-EPS filter to help interpret seismic impedance data. First, seismic impedance is related to the reservoir rock physics characteristics (Ba et al., 2017, 2018; Pang et al., 2019). Second, seismic impedance has higher resolution, which is gained by combining information from well-log data in the process of seismic inversion, compared to seismic amplitude data (AlBinHassan et al., 2006). Especially, the seismic impedance has more explicit geological information. Thin beds are better depicted on impedance sections (Zhang et al., 2014).

We use a seismic impedance cube from real work area to show the application of SA-EPS filter in practice.

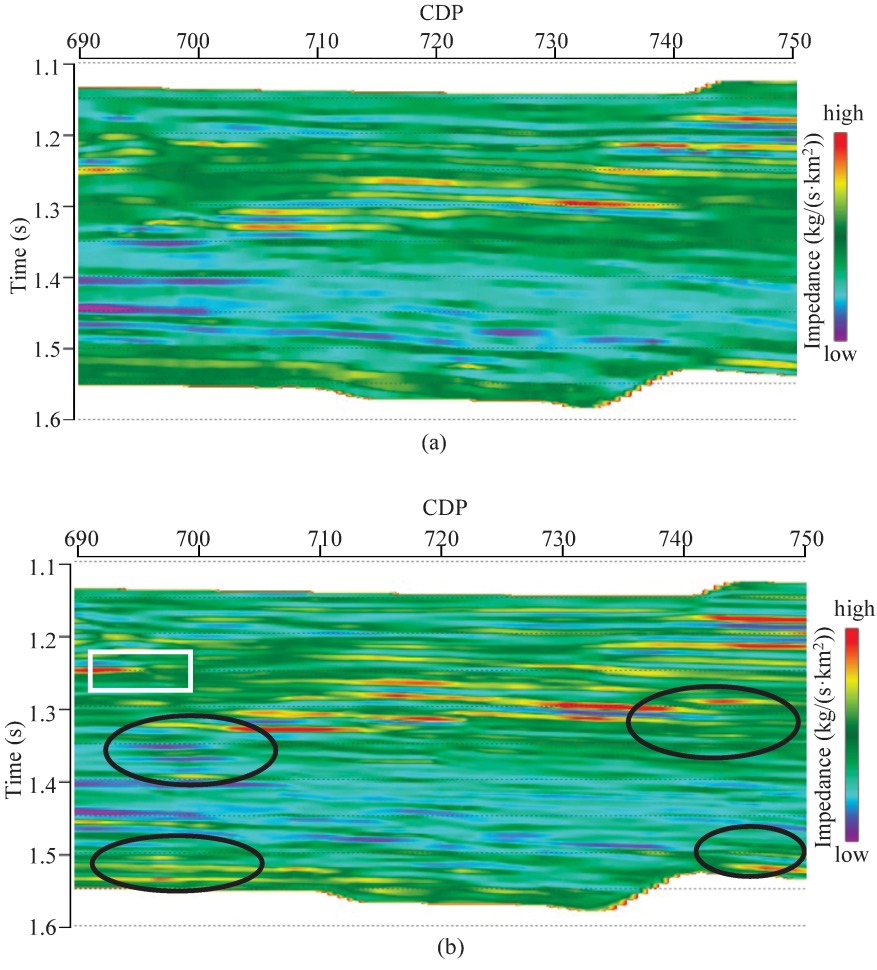

Fig. 9. Comparison between SA-EPS filter and conventional EPS filter performed on real seismic impedance data of inline 560. (a) The filter result of conventional 21-point EPS. (b) The filter result of SA-EPS.

The study area of this seismic impedance cube is located at the middle section of the Kenxi area, Bohai Bay Basin, East China. The target formation develops sandbody reservoirs, which is set of fluvial facies deposition. The lithology includes silty fine sandstone and fine sandstone from coarser below to finer above. The cementation is poor and unconsolidated. The reservoirs' physical quality is good, but changes greatly in the plane. The impedance value of fluvial facies reservoirs is smaller compared to the surrounding rocks.

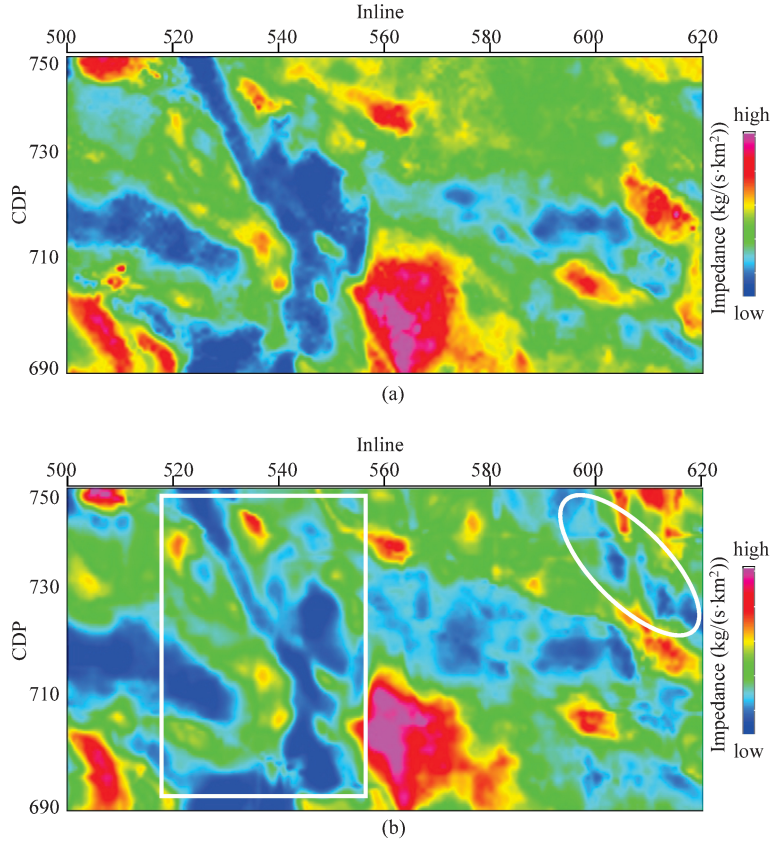

Fig. 10. Comparison of time slice between SA-EPS filter and conventional EPS filter performed on real seismic impedance data of time 1.195s. (a) The filter result of conventional 21-point EPS. (b) The filter result of SA-EPS.

The real seismic impedance cube, which is the result of damped least square inversion (Cooke and Schneider, 1983), contains 121 in-lines from inline500 to inline620, and 61 cross-lines from CDP690 to CDP750. First, the conventional 21-point EPS filter is performed on this real seismic impedance cube. Fig. 9a shows the filter result of 21-point EPS of inline 560. Next, the SA-EPS filter is performed on the real seismic impedance cube. Fig. 9b shows the filter result of SA-EPS of inline 560. We can see that, the fault breakpoint is better defined in Fig. 9b compared to Fig. 9a and the

noise is reduced (e.g., the location at the white rectangle). The interfaces between layers are very obvious and many subtle geologic features stand out in Fig. 9b (e.g., the location at the black ovals).

Further evidence to support SA-EPS filter is shown in time slices (i.e. horizontal sections). Fig. 10 shows a comparison of time slices between the filter results of the conventional EPS and SA-EPS of time 1.195 s. Fig. 10a shows the filter result of conventional EPS, and Fig. 10b shows the filter result of SA-EPS. We can see that, the lineaments of the channel sand are clearer in Fig. 10b (note the location within the white rectangle). Many subtle geologic features (e.g., some tiny channel sand) clearly stand out in Fig. 10b (note the location within the white oval).

In addition, we add another seismic impedance section which crosses a well from another real work area. The filter results of conventional 18-point EPS and SA-EPS are shown in Fig. 11. In Fig. 11, the overlaid log curves are P-wave impedance data from well-log in this work area. From the comparison, we can see that, the filter result of SA-EPS is better-matched with real log curve. Many thin layer interfaces are revealed in Fig. 11b.

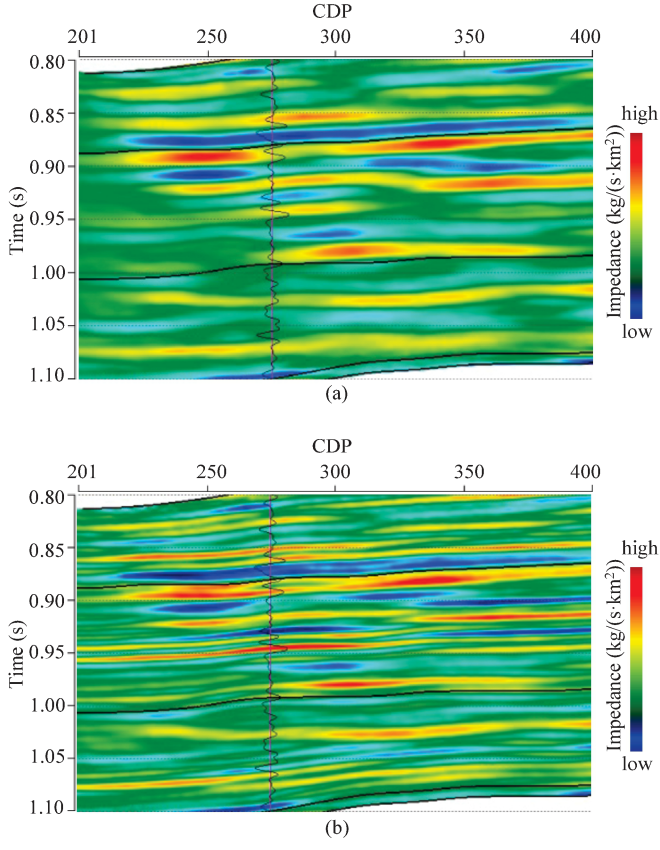

Fig. 11. Comparison between SA-EPS filter and conventional EPS filter performed on a real seismic impedance section crossing a well. (a) The filter result of conventional 18-point EPS. (b) The filter result of SA-EPS.

DISCUSSIONS

To suppress noise while preserve edges of geologic features, lots of method have been developed, such as sparse constraint or total variation regularization in seismic inversion (Claerbout and Muir, 1973; Youzwishen, 2001; Zhang et al., 2014; Dai et al., 2014a, 2016), filter-like methods (e.g. EPS filter, mean or median filter, and structure-oriented filter (Hocker and Fehmers, 2002)), and so forth. In filter-like methods, there is always a trade-off between noise remove and little geologic features preservation. In the exiting literatures, Liu et al., (2009b) proposed a 1D time-varying method to resolve this trade-off in median filter.

In fact, we solve this problem through filter window size scanning. All of the filter-like methods are based on filter window analysis (i.e. analyzing the properties of a series of filter windows), so the principle of SA-EPS filter can be generalized to other filters, such as median filter and structure-oriented filter. However, the disadvantage of filter window size scanning should also be noted. Due to a number of window size needs to be scanned, the computation cost is fairly large. Hence, we propose a fast EPS algorithm. In addition, to accelerate the computation speed, parallel computation is a good solution in practice.

CONCLUSIONS

Edge-preserving smoothing (EPS) method can suppress random noise in seismic cubes while preserve major structural and stratigraphic edges. These structural or stratigrapic discontinuities are very important for seismic interpretaion. However, the conventional EPS filter use fixed filter window size to perform in practice. Hence, the little geological features (e.g., channels, minor fault or thin layers) will be suppressed if their width are smaller than used filter window size. On the other hand, if the filter window size is too small, noise will not be removed sufficiently.

SA-EPS filter proposed in this paper can resolve this trade-off between noise remove and little gologic features preservation through window size scanning. That is: perform a series of EPS filters with different filter window size and find out the best window size which has the smallest window factor at each sample to be filtered. From the applications on both model tests and real data examples show that, the interfaces or edges are obvious in both geologic features in the filter result of SA-EPS; however, the interfaces or edges for some little geologic features (e.g., thin layer, or tiny channel sand) are suppressed in the filter result of conventional EPS. SA-EPS filter is an effective method of random noise remove while geologic features preservation.

ACKNOWLEDGMENTS

This research is supported by the following funds: the National Natural Science Foundation of China (No.41874146), the National Science and Technology Major Project (No.2016ZX05024001-003), and the Initiative Projects for Ph.D. in China West Normal University (No.19E063)." be revised to "the Science and Technology Cooperation Project of CNPC-SWPU Innovation Alliance (No.2020CX010203), the Initiative Projects for Ph.D. in China West Normal University (No.19E063), the Research and Innovation Team of China West Normal University (No.CXTD2020-5), and the National Natural Science Foundation of China (No.41704134).

REFERENCES

AlBinHassan, N.M., Luo, Y. and Al-Faraj M.N., 2006. 3D edge-preserving and applications. Geophysics, 71(4): P5-P11.

Al-Dossary, S., Marfurt, K.J. and Luo, Y., 2002. 3-D edge preserving smoothing for seismic edge detection. Expanded Abstr., 72nd Ann. Internat. SEG Mtg., Salt lake City: 524-527.

Al-Dossary, S. and Marfurt, K.J., 2006. 3D volumetric multispectral estimates of reflector curvature and rotation. Geophysics, 71(5): P41-P51.

Al-Dossary, S. and Marfurt, K.J., 2007. Lineament-preserving filtering.Geophysics,72(1): P1-P8.

Al-Dossary, S. and Wang, Y.E., 2011. Structure-preserving smoothing for 3D seismic attributes. Expanded Abstr., 81st Ann. Internat. SEG Mtg., San Antonio: 1004-1008.

Al-Shuhail, A. and Al-Dossary, S., 2020. Attenuation of Incoherent Seismic Noise. Springer Nature, Switzerland.

Ba, J., Xu, W., Fu, L., Carcione, J.M. and Zhang, L., 2017. Rock anelasticity due to patchy-saturation and fabric heterogeneity: A double double-porosity model of wave propagation. J. Geophys. Res., Solid Earth, 122: 1949-1976.

Ba, J., Zhang, L., Wang, D., Yuan, Z., Cheng, W., Ma, R. and Wu, C., 2018. Experimental analysis on P-wave attenuation in carbonate rocks and reservoir identification. J. Seismic Explor., 27: 371-402.

Claerbout, J.F. and Muir, F., 1973. Robust modeling with erratic data. Geophysics, 38: 826-844.

Cooke, D.A. and Schneider, W.A., 1983. Generalized linear inversion of reflection seismic data. Geophysics, 48: 665-676.

Dai, R., Zhang, F., Liu, H. and Li, C., 2014a. Non-Linear Pre-Stack Seismic AVA Inversion Based on Bayesian Theory Using Successive Iteration Method. J. Jilin Univ., Earth Science Ed., 44: 2026-2033.

Dai, R., Zhang, F., Liu, H., Wang, P. and Zhang Z., 2014b. Method of AVA inversion using replacing parameters. Expanded Abstr., 84th Ann. Internat. SEG Mtg., Denver: 559-563.

Dai, R., Zhang, F. and Liu, H., 2015. AVA inversion using replacing parameters method for pre-stack seismic data. Prog. Geophys., 30: 261-266.

Dai, R., Zhang, F. and Liu, H., 2016. Seismic inversion based on proximal objective function optimization algorithm. Geophysics, 81(5): R237-R246.

Fehmers, G.C. and Hocker, C.F.W., 2003. Fast structural interpretation with structure-oriented filtering. Geophysics, 68: 1286-1293.

Halpert, A.D., 2012. Edge-preserving smoothing for segmentation of seismic images. Expanded Abstr., 82nd Ann. Internat. SEG Mtg., Las Vegas: 1-5.

Hocker, C. and Fehmers, G., 2002. Fast structural interpretation with structure-oriented filtering. The Leading Edge, 21: 238-243.

Liu, Y., Luo, Y. and Wang, Y., 2009a. Vector median filter and its applications in geophysics. Expanded Abstr., 79th Ann. Internat. SEG Mtg., Houston: 3342-3345.

Liu, Y., Liu, C. and Wang, D., 2009b. A 1D time-varying median filter for seismic random, spike-like noise elimination. Geophysics, 74(1): V17-V24.

Liu, Y. and Luo, Y., 2012. Reducing random noise in vector field using vector median filter. Expanded Abstr., 82nd Ann. Internat. SEG Mtg., Las Vegas: 1-5.

Luo, Y., Marhoon, M., Al-Dossary, S. and Alfaraj, M., 2002. Edge-preserving smoothing and applications. The Leading Edge, 21: 136-158.

Marfurt, K.J., 2006. Robust estimates of 3D reflector dip and azimuth. Geophysics, 71(4): P29-P40.

Misra, S. and Sacchi, M.D., 2008. Global optimization with model-space preconditioning: Application to AVO inversion. Geophysics, 73(5): P71-P82.

Pang, M., Ba, J., Carcione, J.M., Picotti, S., Zhou, J. and Jiang, R., 2019. Estimation of porosity and fluid saturation in carbonates from rock-physics templates based on seismic Q. Geophysics, 84 (6): M25-M36.

Wang, Z., Yin, C., Fan, T. and Lei, X., 2012. Seismic geomorphology of a channel reservoir in lower Minghuazhen Formation, Laizhouwan subbasin, China. Geophysics, 77(4): B187-B195.

Youzwishen, C.F., 2001. Non-linear sparse and blocky constraints for seismic inverse problems. University of Alberta.

Zhang, F., Dai, R. and Liu, H., 2014. Seismic inversion based on L1-norm misfit function and total variation regularization. J. Appl. Geophys., 109: 111-118.

Zhang, F., Li, D. and Dai, R., 2015a. Seismic inversion based on edge preserving smooth regularization. J. China Univ. Min. Tech., 44: 255-261.

Zhang, F., Dai, R. and Liu, H., 2015b. High order approximation for scattering matrix in layered elastic medium and its application in pre-stack seismic inversion. J. Petrol. Sci. Engineer., 131: 210-217.

Zhang, F. and Dai, R., 2016. Nonlinear inversion of pre-stack seismic data using variable metric method. J. Appl. Geophys., 129: 111-125.